Molecular Structure of the Gaseous Metal Carbonyl Hydrides of Manganese, Iron, and Cobalt

E. A. McNeill and F. R. Scholer*

Contribution from the Department of Chemistry, Baker Laboratory, Cornell University, Ithaca, New York 14853. *Received August 23, 1976*

Abstract: The molecular structure for $HMn(CO)_5$, $H_2Fe(CO)_4$, and $HCo(CO)_4$ has been investigated by gas-phase electron diffraction. The results for $HMn(CO)_5$ are indistinguishable from the neutron diffraction study. Within their combined experimental errors, the electron diffraction value for the Mn-H distance (1.576 (18) Å) is comparable to the neutron diffraction value (1.601 (16) Å). In $H_2Fe(CO)_4$ the $Fe(CO)_4$ group has C_{2v} symmetry with a configuration intermediate between octahedral and tetrahedral geometries. The hydrogen atoms are cis, with an ∠H-Fe-H = 100 (10)°. The ∠C-Fe-C angles for the axial and equatorial sets are 148.5 (1.5) and 96.0 (0.6)°, respectively. The Fe-H distance is 1.556 (21) Å. The structure $HCo(CO)_4$ has C_{3v} symmetry, with the hydrogen directly bonded to the cobalt at a distance of 1.556 (18) Å.

The syntheses of the metal carbonyl hydrides of manganese, cobalt, and iron were reported in 1931,[1] but the structures of the latter two were not established unambiguously either with respect to the geometry of the metal carbonyl core or to the location of the hydrogen; the structure of $HMn(CO)_5$ was determined by neutron diffraction analysis.[2] An early electron diffraction investigation by Ewens and Lister[3] suggested the $Co(CO)_4$ group had tetrahedral symmetry with the hydrogen atom bonded to one of the oxygens. Recent spectral data by Edgell et al.[4] as well as broad-line NMR studies[5] indicated that $HCo(CO)_4$ was a distorted trigonal bipyramid, with the hydrogen bonded directly to the metal. Based on spectral studies a cis-octahedral geometry has been proposed for $H_2Fe(CO)_4$,[6-8] but definitive structural data are not available. The molecular spectra of $HMn(CO)_5$[9-15] suggest a C_{4v} symmetry for the $Mn(CO)_5$ moiety, but do not provide values for the Mn-H distance. Combined x-ray[16] and neutron diffraction[2] results have firmly established that the Mn-H distance is 1.601 (16) Å. A complete review of metal-hydride chemistry is available.[17]

This electron diffraction study was undertaken to determine the structure of the metal carbonyl hydrides and to determine the mean distance between the metal and hydrogen atoms.

Experimental Section and Data Reduction

$HMn(CO)_5$. Under an inert atmosphere, 0.500 g (1.35 mmol) of freshly sublimed $Mn_2(CO)_{10}$ was dissolved in 25 mL of freshly distilled tetrahydrofuran (THF) and stirred over a Na/Hg amalgam (0.0622 g (2.70 mmol) in 50 g of Hg) for 3 h. The solution was filtered and the solvent distilled off. The resulting green solid was heated to 60 °C and maintained at that temperature under a partial vacuum (<1 μ) for 3 days. The reaction vessel was cooled to 0 °C and 30 mL of degassed 0.1 M H_3PO_4 was added. The volatiles were passed through a drying tube filled with P_2O_5 and trapped at −78 °C. The $HMn(CO)_5$ was identified by infrared spectrum. The infrared spectrum showed no indication of THF or CO_2. This sample of $HMn(CO)_5$ was used without further purification. The diffraction patterns were recorded with the Cornell instrument[18] on Kodak Electron Image plates,[19] at wavelengths of 0.054 927 and 0.044 202 Å, and nozzle-to-plate distances (L) of 285.7 mm (p = 12-59 Å^{-1}) and 127.0 mm (p = 47-170 Å^{-1}), respectively ($p = (50/\lambda)\sin\theta/2$). The sample reservoir was maintained at 25 °C. Several MgO patterns were taken concurrently to calibrate the magnitude of L.[20] The radial optical density functions were recorded with a double-beam Jarrel-Ash densitometer, interfaced with a digital recorder. The optical densities were measured at 0.100- and 0.150-mm intervals for the short and long distances, respectively, thus providing a minimum of four data points for each p value. The densities were converted to relative intensities, interpolated at integral values of p, corrected for nonflatness of the focal plane, and averaged. Five data sets from each of two plates were used for the long distance and four data sets from each of three plates were used for the short distance. Because of the relatively large spread in atomic numbers in the metal carbonyl hydrides, the phase shift difference, $\Delta\eta_{ij}$, between the metal and all the other atoms is large compared to differences between hydrogen, carbon, and oxygen. The nonnuclear scattering by the metal carbonyl hydrides is about 10% of the total scattering for $p > 30$ Å^{-1}, because the rapidly changing $\cos(\Delta\eta_{ij})$ term reduces the nuclear contribution to the scattering. In turn, because the nonnuclear contribution is appreciable in hydride-metal carbonyls, reliable values for the form factors, f_i, and phase shifts, η_i, are essential. The magnitudes used in this investigation were interpolated to the appropriate voltage, i.e., wavelength, from the tables of Schafer et al.[21] Analytic expressions were then fitted to the interpolated values to minimize computer core space. For the form factors, two different analytical expressions were used depending upon the p range:

$$f(p) = A\exp(-ap^2) + B\exp(-bp) + C \qquad 4 \le p \le 80 \quad (1)$$

and

$$f(p) = A'p\exp(-a'p) + B'\exp(-b'p) + C' \qquad 60 \le p \le 200 \quad (2)$$

For first-row elements, expression 1 adequately fits the whole range of p between 4 and 200,[22] but for larger atomic elements such as cobalt, iron, and manganese, the analytical expression (eq 1) decreases much too rapidly. For heavy atoms, the expression (eq 2) significantly improves the fit.[23] The interval $60 < p < 80$ was chosen as the splice-over-range because that was the suitable splice-over-range for the two data sets. Hence, in practice, expression 1 represents the low voltage, low angle form factors while expression 2 represents the high voltage, wide angle form factors. The analytical expression for the phase shifts, η_i, took the same form for both the low and high voltage data sets, being represented by a fourth order polynomial,

$$\eta_i(p) = a + bp + cp^2 + dp^3 + ep^4 \quad (3)$$

The same ranges of fit as for the form factors were used. The electron diffraction theoretical and experimental expressions were spliced in the manner previously described.[22] The procedure for structural analysis has been described elsewhere.[24-26]

$H_2Fe(CO)_4$. The sample was prepared by the procedure of Farmery et al.[7] and purified by repeated fractionation through two −63 °C slush baths, and trapped at −196 °C. The latter was warmed to −96 °C, and the contents were pumped on to reduce the pressure to less than 1 μ, thereby removing any CO_2. The trap was then quickly taken from the vacuum line and attached directly to the Cornell apparatus and again degassed. The trap was then placed in a −45 °C slush bath, and diffraction photographs were taken as soon as any vapor pressure was observed. Several attempts were made using a −35 °C slush, but about 8-10% decomposition resulted in excess CO and H_2, as expected.[27] Photographs were recorded at wavelengths of 0.054 927 and 0.044 202 Å, and nozzle-to-plate distances of 285.7 mm (p = 10-59 Å^{-1}) and 127.4 mm (p = 30-170 Å^{-1}), respectively. Several calibrating MgO patterns were taken concurrently. Three data sets from

* Author to whom correspondence should be addressed at Industrial Chemical Division, FMC Corporation, Princeton, N.J. 08540.

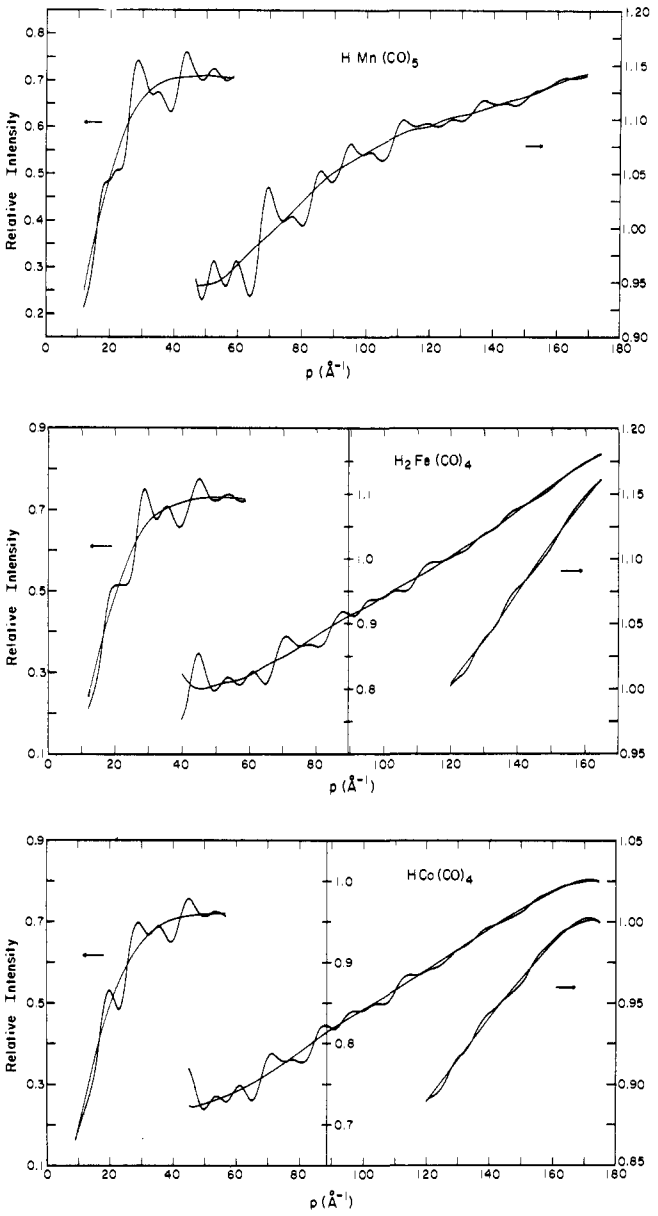

Figure 1. The relative scattered intensity and refined background curves for (top) $HMn(CO)_5$ (splice point p = 55 Å^{-1}), (center) $H_2Fe(CO)_4$ (splice point p = 55 Å^{-1}), and (bottom) $HCo(CO)_4$ (splice point p = 47 Å^{-1}). The high angle portions of the curves for $H_2Fe(CO)_4$ and $HCo(CO)_4$ are presented with an expanded scale.

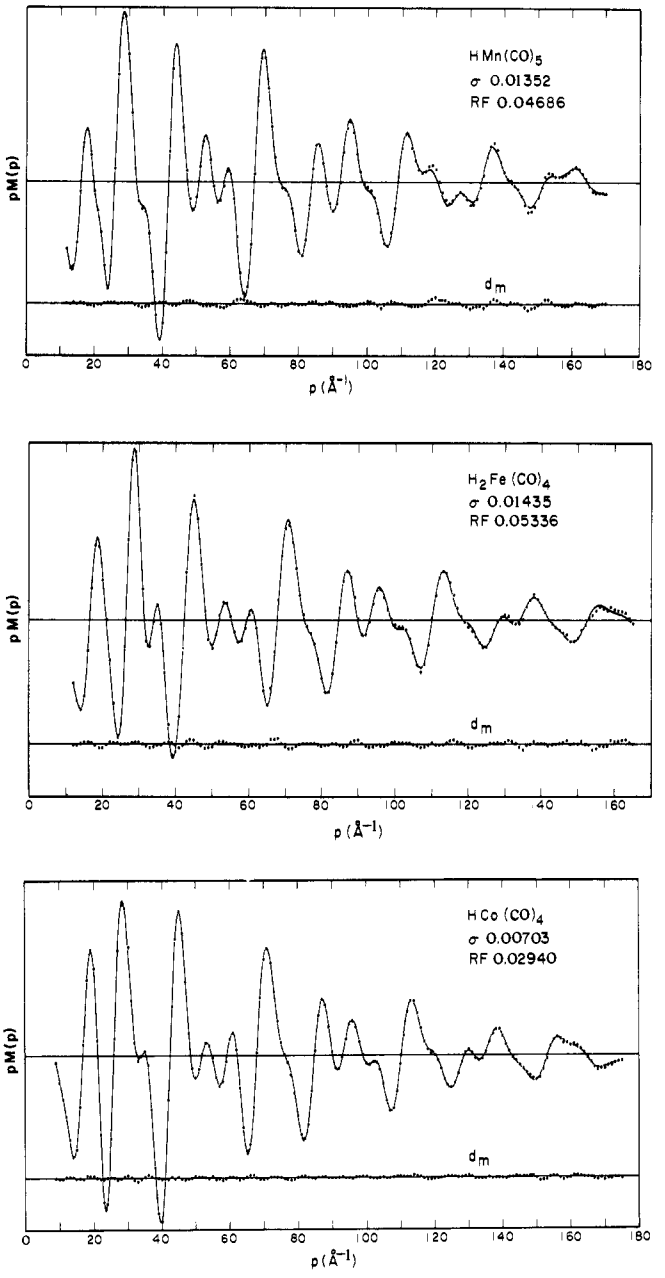

Figure 2. The reduced experimental molecular scattering curves, $pM(p)$ (dots), the theoretical $pM(p)$ (solid line), and the dashed difference curve, d_m (experimental minus theoretical), for (top) $HMn(CO)_5$, (center) $H_2Fe(CO)_4$, and (bottom) $HCo(CO)_4$.

each of three plates were averaged for the long distance and four data sets from each of three plates were used for the short distance. The procedure for analysis was the same as that followed for $HMn(CO)_5$.

$HCo(CO)_4$. The sample was prepared by the procedure of Steinberg et al.[28] and purified by vacuum distillation at −45 °C. Sectored gas-phase electron diffraction photographs were recorded with the Cornell apparatus, while the sample was maintained at −35 °C. The elapsed time between the synthesis of the sample and recording of the data was less than an hour. Sectored patterns were photographed with wavelengths of 0.056 519 and 0.044 202 Å, and sample-to-plate distances of 284.9 mm (p = 9-54 Å^{-1}) and 127.4 mm (p = 40-173 Å^{-1}), respectively. The distances were established from concurrently recorded MGO patterns. Three data sets from each of three plates for the long distance and four data sets from each of three plates for the short distance were used. The procedure for analysis was the same as that followed for $HMn(CO)_5$.

Trial Structures and Refinement. $HMn(CO)_5$. The relative scattered intensity as a function of angle p (Å^{-1}) has been plotted along with the refined background in Figure 1. The reduced scattered intensity $pM(p)$ as a function of p (Å^{-1}) is shown in Figure 2. On the basis of an excellent neutron diffraction structure,[2] the molecular configuration was assigned to C_{4v} symmetry, with the hydrogen bonded directly to the metal. This structure is completely specified by only six geometric parameters: the Mn-H, Mn-C_{eq}, Mn-C_{ax} distance, the average C-O distance, and the angles H-Mn-C_{eq} and Mn-C_{eq}-O_{eq}. Eighteen additional parameters are required to describe the root mean square amplitude of vibration between atom-atom pairs, assuming that l(Mn—C_{ax}) is equal to l(Mn—C_{eq}) and that l(Mn···O_{ax}) is equal to l(Mn—O_{eq}). The molecular configuration and atomic numbering scheme are shown in Figure 3. Initial estimates of the l_{ij}'s were based on the electron diffraction structures of $Fe(CO)_5$[29] and $Fe(CO)_4$-C_2F_4.[30] Other values were obtained from trial radial distribution curves. In the final refinement of the $pM(p)$ curve, all six geometric parameters and the l_{ij}'s for the C—O, Mn—C, and Mn···O were varied concurrently and the computation converged. The final standard deviation and R factor[31] were 0.013 61 and 0.047 07, respectively.

The final radial distribution curve is shown in Figure 4. The first peak at 1.1 Å is due to the C-O distance and the large peak at 1.8 η

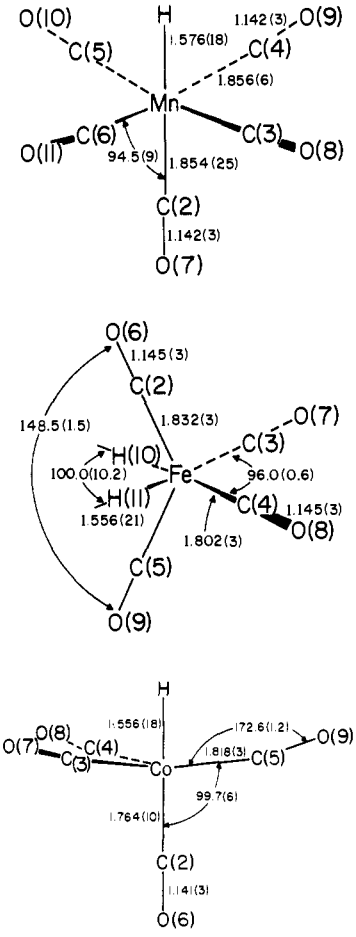

Figure 3. The molecular configuration and atomic numbering scheme for (top) $HMn(CO)_5$, (center) $H_2Fe(CO)_4$, and (bottom) $HCo(CO)_4$.

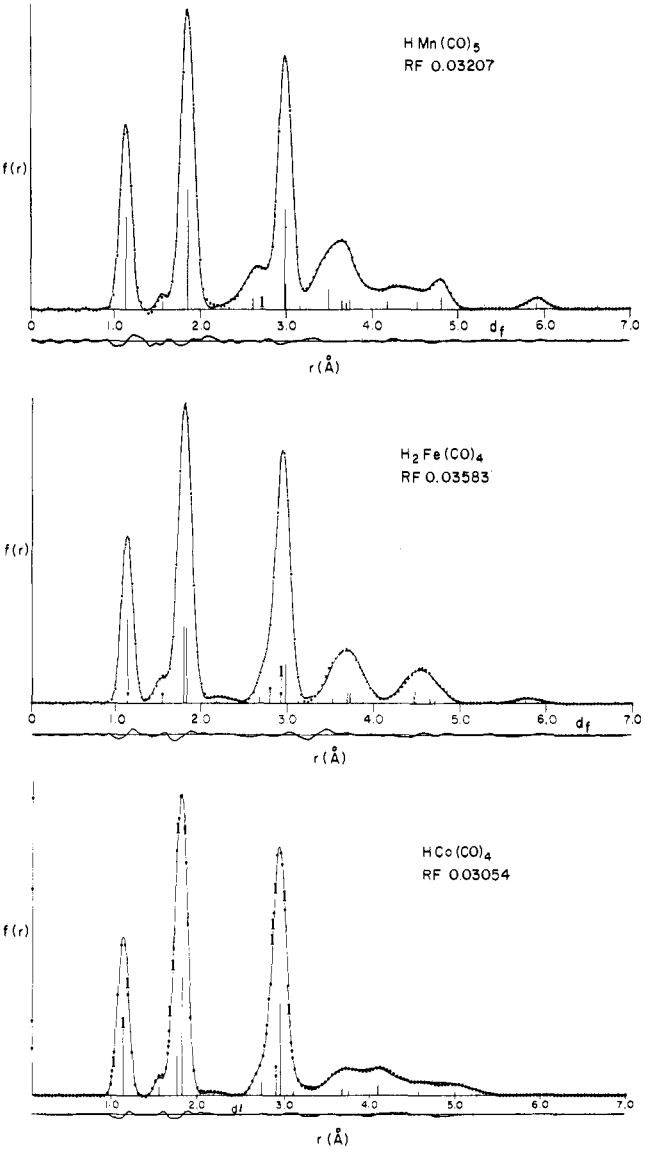

Figure 4. The refined experimental radial distribution curve (dots), the theoretical radial distribution curve (solid line), and the difference curve, d_f (experimental minus theoretical), for (top) $HMn(CO)_5$, (center) $H_2Fe(CO)_4$, and (bottom) $HCo(CO)_4$.

is a superposition of the two Mn-C distances. The small peak at 1.58 Å is assigned to the Mn-H distance. The rounded peak at 2.8 Å is the superposition of the $C_2\cdots C_3$ and $C_3\cdots C_4$ peaks while the sharp peak at 3.0 Å is the superposition of Mn···O distances. The final values of the geometric and thermal parameters along with the resultant r_{ij}'s are listed in Tables I and II. The reduced experimental molecular intensity curve along with the difference curve is shown in Figure 2.

$H_2Fe(CO)_4$. The relative scattered intensity as a function of angle p (Å^{-1}), and the refined background, is plotted in Figure 1. The reduced scattered intensity $pM(p)$ as a function of p (Å^{-1}) is shown in Figure 2. In the initial stages of the analysis the hydrogens were deleted from the model, and four symmetries, C_{2v}, Td, D_{2d}, and D_{4h}, were tested for the $Fe(CO)_4$ fragment. These are illustrated in Figure 5. Initial estimates for the geometric and thermal parameters were taken from the literature.[29,30] In all the models, all the C—O distances and l_{ij}'s were grouped, as were the l(Fe—C) and l(Fe···O). It became immediately apparent from the radial distribution curve (Figure 4) that the Td and D_{4h} models with equivalent Fe-C distances were unsatisfactory. Further refinement showed that the C_{2v} symmetry was clearly favored over the other three. The C_{2v} and D_{2d} models were assigned the same number of thermal parameters. Only one additional parameter, a geometrical one, was introduced in going from D_{2d} to C_{2v} symmetry. On applying Hamilton's ratio of R factors,[32] the D_{2d} model was eliminated at the 99.5% confidence level. The R factor for D_{2d} is above 0.0904. The $pM(p)$ R factors and standard deviations for the "best fit" models for the four assumed symmetries of the $Fe(CO)_4$ unit are listed in Figure 5.

The angles between the carbonyls are 96 and 148°, about halfway between an octahedron with the two hydrogens cis, and a bicapped tetrahedron with the two hydrogens at the caps. For the C_{2v} model, nine geometric parameters are needed: the C-O average distance, Fe-C_{ax} distance, Fe-C_{eq} distance, Fe-H distance, and the angles $\angle HFeH$, $\angle C_{eq}FeC_{eq}$, $\angle C_{ax}FeC_{ax}$, $\angle FeC_{ax}O$, and $\angle FeC_{eq}O$. The corresponding atomic configuration and numbering scheme are presented in Figure 3. During least-squares calculations of the $pM(p)$ curve, all the geometric and thermal parameters were varied in a cyclic sequence until convergence was obtained. In the final refinement step, all the geometric parameters except $\angle FeC_{ax}O$ and $\angle FeC_{eq}O$ were varied, along with the C—O, FeC, and Fe···O l_{ij}'s. The computation converged, and the best values are summarized in Table I. A list of the internuclear distances and their respective l_{ij}'s is presented in Table II. The final $pM(p)$ standard deviation and R factor were 0.014 43 and 0.053 64, respectively.

In the final radial distribution curve, shown in Figure 4, the first peak at 1.1 Å is assigned the C-O distance, and the small peak at 1.6 Å is assigned the Fe-H distance, while the large one at 1.8 Å is a superposition of the two Fe-C distances. The small peak at 2.2 Å is a superposition of H···H, H···C_{ax}, and H···C_{eq} distances, with the peak at 2.7 Å assigned to the different C···C distances. The peak at 3 Å is the superposition of Fe···O distances; the peak at 5.7 Å is assigned the $O_{ax}\cdots O_{ax}$. For both sets of carbonyls the oxygens are bent somewhat toward the hydrogens.

$HCo(CO)_4$. The relative scattered intensity as a function of p and the refined background are shown in Figure 1. In the models considered in this study, all C—O distances were assumed equal, as were all l(C—O), l(Co—C), and l(Co···O). The $pM(p)$ curve vs. p is presented in Figure 2. In the initial trials two models of the $Co(CO)_4$ fragment were assumed, one of C_{2v} symmetry and the other C_{3v}; the hydrogens were omitted. While both fitted the observed patterns well,

Table I. Geometrical Parameters[a]

$HMn(CO)_5$		$H_2Fe(CO)_4$		$HCo(CO)_4$	
Parameter	Value	Parameter	Value	Parameter	Value
$C-O_{av}$	1.142 (3)	$C-O_{av}$	1.145 (3)	$C-O_{av}$	1.141 (3)
Mn-H	1.576 (18)	Fe-H	1.556 (21)	Co-H	1.556 (18)
$Mn-C(2)_{ax}$	1.854 (30)	$Fe-C(2)_{ax}$	1.832 (3)	$Co-C_{ax}$	1.764 (10)
$Mn-C(3)_{eq}$	1.856 (6)	$Fe-C(3)_{eq}$	1.802 (3)	$Co-C_{eq}$	1.818 (3)
$\angle C_{ax}-Mn-C_{eq}$	94.53 (84)	$\angle C(2)_{ax}-Fe-C(5)_{ax}$	148.5 (1.5)	$\angle C_{ax}-Co-C_{eq}$	99.7 (6)
$\angle Mn-C_{eq}-O_{eq}$	190.06 (1.29)	$\angle C(4)_{eq}-Fe-C(5)_{eq}$	96.0 (0.6)	$\angle Co-C_{eq}-O_{eq}$	172.6 (1.2)
		$\angle Fe-C(4)_{eq}-O(8)$	165.5 (2.1)		
		$\angle Fe-C(2)_{ax}-O(6)$	176.2 (3.6)		
		H-Fe-H	100.0 (10.2)		

[a] The distances are in angstroms and the angles in degrees. The calculated uncertainties are given in parentheses and refer to the last numbers given. These uncertainties are three times the least-squares standard deviation or 0.15% of the quantity listed, whichever is greater.[26]

Table II. Atom Pair Distances and Root Mean Square Amplitudes of Vibration (Å)[g]

Atom pair	r_{ij}	l_{ij}	Atom pair	r_{ij}	l_{ij}	Atom pair	r_{ij}	l_{ij}
$C-O_{av}$	1.142	0.041 (1)	$C-O_{av}$	1.145	0.041 (2)	$C-O_{av}$	1.141	0.039 (1)
Mn-H	1.576	0.040 (25)	Fe-H	1.556	0.060 (40)	Co-H	1.556	0.030 (20)
Mn-C(2)	1.854	0.059 (1)[a]	Fe-C(3)	1.802	0.053 (3)[a]	Co-C(2)	1.764	0.045 (30)[a]
Mn-C(3)	1.856	0.059 (1)[a]	Fe-C(2)	1.832	0.053 (3)[a]	Co-C(3)	1.818	0.045 (30)[a]
H-C(3)	2.331	0.191 (60)	H-C(2)	2.187	0.176 (50)[b]	H-C(3)	2.186	0.114 (40)
C(3)-C(4)	2.615	0.140 (20)	C(3)-C(4)	2.678	0.050 (21)	C(3)-C(4)	3.105	0.183 (30)
C(2)-C(3)	2.724	0.108 (12)	C(2)-C(3)	2.793	0.078 (12)	C(2)-C(3)	2.738	0.073 (60)
Mn-O(8)	2.986	0.058 (2)[b]	Fe-O(7)	2.924	0.052 (3)[c]	Co-O(7)	2.954	0.050 (20)[b]
Mn-O(7)	2.996	0.058 (2)[b]	Fe-O(6)	2.975	0.052 (3)[c]	Co-O(6)	2.905	0.050 (20)[b]
H-O(8)	3.163	0.081[f]	H(10)-O(7)	2.971	0.120[f]	H-O(7)	3.025	0.102 (40)
H-C(2)	3.420	0.100[f]	H(10)-C(4)	3.356	0.100 (21)	H-C(2)	3.312	0.190[f]
C(3)-O(9)	3.497	0.152 (10)	C(3)-O(8)	3.731	0.151 (33)	C(3)-O(9)	3.755	0.212 (20)
C(3)-O(7)	3.646	0.173 (15)	C(3)-O(6)	3.725	0.164 (69)	C(3)-O(6)	3.677	0.133 (12)
C(3)-C(5)	3.697	0.062 (15)	C(2)-C(5)	3.526	0.061 (30)			
C(2)-O(8)	3.737	0.173 (15)	C(2)-O(7)	3.692	0.151 (33)	C(2)-O(7)	4.100	0.176 (13)
O(8)-O(9)	4.178	0.217 (40)	O(6)-O(7)	4.467	0.148 (18)[d]	O(8)-O(7)	4.994	0.224 (22)
O(7)-O(8)	4.527	0.212 (40)	O(7)-O(8)	4.709	0.131 (30)[e]	O(7)-O(6)	4.570	0.220 (18)
H-O(7)	4.563	0.140[f]	H(10)-O(8)	4.479	0.148 (18)[d]	H-O(6)	4.460	0.100[f]
C(3)-O(10)	4.811	0.084 (12)	C(2)-O(9)	4.652	0.131 (30)[e]			
O(8)-O(10)	5.908	0.103 (30)	O(9)-O(6)	5.765	0.134 (80)			
			H(10)-C(3)	2.211	0.176 (50)[b]			
			H-H	2.384	0.100[f]			
			H-O(6)	3.131	0.135[f]			

[a-e] Assumed equal. [f] Value assumed. [g] The calculated uncertainties are given in parentheses and refer to the last numbers given. These uncertainties are three times the least-squares standard deviation. The l_{ij}'s are grouped, where possible, according to structural type rather than in increasing values of r_{ij}.

the C_{3v} symmetry is clearly favored upon careful comparison of the $pM(p)$ curve. Introduction of the hydrogen along the C_2 axis in the C_{2v} model substantially reduced the standard deviation and R factor. However, upon introducing the hydrogen on the C_3 axis in the C_{3v} model, the standard deviation and R factor are more than halved in comparison to the C_{2v} model. It is interesting to speculate regarding three other possibilities for the hydrogen position: one of the other three faces, between two of the three equatorial carbons, and between an equatorial carbon and the unique axial carbon. The standard deviations and R factors for all the models are listed in Figure 6. While hydrogen is located on a face of the C_{3v} fragment, it is most favored to be on the C_3 axis. The result is a trigonal bipyramid with the hydrogen in the axial position, as shown in Figure 3.

In the trigonal bipyramid model, six geometric parameters are needed to specify the atomic positions: C-O (average distance), Co-C_{eq}, Co-C_{ax}, and Co-H distances, and the angles $\angle$Co-C_{eq}-O and $\angle$H-Co-C_{eq}. Fifteen l_{ij}'s were required to specify the atom pair vibrations. All geometric and vibrational parameters were varied. In the final refinement step, all the geometric parameters and (C—O), (Co—C), and (Co···C) l_{ij}'s were varied. A list of the internuclear distances and l_{ij}'s is presented in Table II.

The final radial distribution curve is presented in Figure 4. The first peak at 1.1 Å is assigned the C-O distance. The next peak at 1.6 Å is due to the Co-H distance, while the sharp peak at 1.8 Å is the superposition of the two Co-C distances. The small isolated peak at 2.1 Å is assigned the H···C distance while the large peak at 2.9 Å is the superposition of C···C and Co···O distances. The difference curve is denoted by d_f.

Discussion

In the gas phase the structure of $HMn(CO)_4$ has C_{4v} symmetry; it is not significantly different from the geometry of either α- or β-$HMn(CO)_4$ found in the solid state by crystallographic methods. The principal intramolecular bond distances and angles are shown in Table I. In this compound the equatorial carbonyl groups bend slightly toward the hydrogen ligand and away from the axial carbonyl. Examination of previously determined structures of $XMn(CO)_5$ complexes, assembled in Table III, shows that the Mn-C_{ax} distance is consistently shorter than Mn-C_{eq} by 0.02–0.05 Å. The electron diffraction values are not compatible with a difference of this magnitude (combined error limits = 0.03 Å). Several explanations have been advanced for this trend.[37-39]

The Mn-H bond distance of 1.576 (18) Å is within the uncertainty of the distance determined by neutron diffraction and, as noted by La Placa et al.,[2] "is in reasonable agreement

Table III. Axial vs. Equatorial Mn-C Bond Lengths (Å) in $XMn(CO)_5$ Complexes

Compound	Technique	$Mn-C_{ax}$	$Mn-C_{eq}$ (av)	Eq − ax	Ref
α-$HMn(CO)_5$	X-ray	1.821 (9)	1.840 (5)	0.019 (10)	16
β-$HMn(CO)_5$	X-ray	1.824 (17)	1.853 (7)	0.029 (18)	2
β-$HMn(CO)_5$	Neutron	1.822 (12)	1.853 (12)	0.031 (17)	2
$(CO)_5Mn-Mn(CO)_5$	X-ray	1.792 (14)	1.831 (9)	0.039 (17)	33
$(CO)_5Mn-Fe(CO)_4-Mn(CO)_5$	X-ray	1.805 (10)[a]	1.855 (10)[a]	0.050 (14)	34
$CH_3Mn(CO)_5$	Electron	1.820[b]	1.860 (10)	0.040 (10)	35
$F_3SiMn(CO)_5$	Electron	1.856 (8)	1.876 (8)	0.020 (12)	36
$HMn(CO)_5$	Electron	1.852 (30)	1.854 (6)	0.002 (12)	This work

[a] Error estimate from ref 2. [b] This value is assumed because of limited data, 1.75 s, 19.875 $Å^{-1}$.

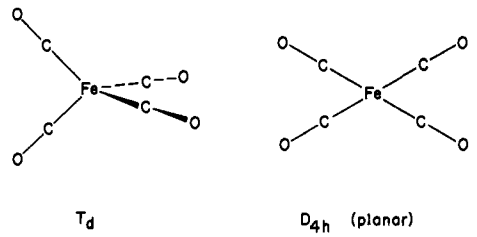

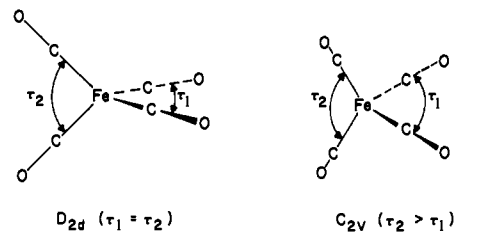

Symmetry	Standard Deviation	R factor
T_d	0.09238	0.26676
D_{4h}	0.07510	0.20377
D_{2d}	0.03783	0.11757
C_{2v}	0.02349	0.08777

Figure 5. The four symmetries of the $Fe(CO)_4$ fragments and their corresponding standard deviations and R factors calculated from the $pM(p)$ curve.

Model	Standard Deviation	R factor
$C_{3v}Co(CO)_4$	0.015217	0.059246
$C_{2v}Co(CO)_4$	0.017092	0.065084
$C_{3v}HCo(CO)_4$	0.007038	0.028702
$C_{2v}HCo(CO)_4$	0.013267	0.049686
$C_{3v}Co(CO)_4$ + H in ax edge[(ae)]	0.0100835	0.038709
$C_{3v}Co(CO)_4$ + H in eq edge[(ee)]	0.0119404	0.044227
$C_{3v}Co(CO)_4$ + H in one[(f)] of three different faces	0.007718	0.030467

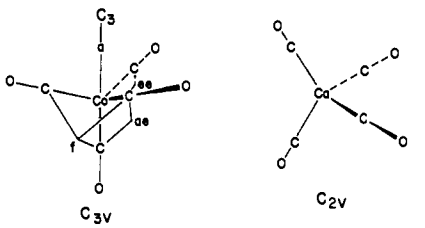

Figure 6. The different models of $HCo(CO)_4$ and their corresponding standard deviations and R factors calculated from the $pM(p)$ curve.

with that which can be predicted from the sums of covalent radii." However, the anomalously short Mn-H bond length of 1.42 Å determined by a prior electron diffraction study[14] was a source of concern. Comparison of our radial distribution curve with that reported previously[14] indicates that the peak at 1.42 Å previously assigned to the Mn-H distance is absent. This may have been a spurious peak due to an impurity. The good agreement between this study and the neutron diffraction results indicates that adequate sample purification is essential for reliable electron diffraction studies.

Four models were considered for the $Fe(CO)_4$ fragment (Figure 5). The favored C_{2v} model (Figure 3) is described by two angles, τ_1 and τ_2, which are 96 (0.6)° and 148.5 (1.5)°, respectively. A theoretical analysis of the $M(CO)_4$ fragment suggests that the preferred geometry for a low-spin d^8 $M(CO)_4$ system has D_{2d} symmetry, with $\tau_1 = \tau_2 \cong 150°$.[39] On the basis of IR matrix-isolated spectra $Fe(CO)_4$ was assigned C_{2v} symmetry,[41] but it is suspected that the iron is in a high-spin state.[39] Geometric distortion of $M(CO)_n$ fragments by a hydrogen atom is now well documented from crystallographic studies on the $HMn(CO)_5$.[2] Theories based on either steric or electronic arguments[39] have been developed. The latter predict that in dihydrides of the type H_2FeL_4, the FeL_4 core should show distortion toward the tetrahedral limit, assuming the H^- ligand is a good σ donor. This arrangement of carbonyl ligands about the Fe is very similar to the arrangement found for the phosphorus atoms in $H_2Fe[(C_6H_5)P(OC_2H_5)_2]_4$ by x-ray crystallography.[40] In $H_2Fe(CO)_4$ the axial carbonyl groups (C(2), C(5)) are bent away from the octahedral configuration toward a tetrahedral configuration. The C(2)-Fe-C(5) angle (τ_2) is 148.5°, while the angle for the equatorial carbonyl groups (τ_1), C(3)-Fe-C(4), is 96.0°. The corresponding angles for the P-Fe-P bond are 136.7° and 102.3°, respectively. The $Fe-C_{ax}$ distance is longer than the $Fe-C_{eq}$ distance (1.832 vs. 1.802 Å); the difference is five times larger than the combined experimental error. However, in the $H_2Fe[(C_6H_5)P(OC_2H_5)_2]_4$ the $Fe-P_{ax}$ distance is slightly shorter than the $Fe-P_{eq}$ (2.134 vs. 2.153 Å). The H(10), H(11), Fe, C(3), and C(4) atoms appear to be coplanar. The H-Fe-H angle of 100.0° corresponds to the angle (88°) in the phosphite structure, as does the Fe-H distance, at 1.556 (2) Å.

The electron diffraction structure of $HCo(CO)_4$ is a distorted trigonal bipyramid, with C_{3v} symmetry and the hydrogen bonded directly to the cobalt (Figure 6). The C_{2v} model is clearly a statistically poorer fit. The $C_{ax}-Co-C_{eq}$ angle of 99.7° was proposed on the basis of infrared spectra[4] (101 ± 1.5°); it is halfway between that present in a trigonal bipyramid (σ = 90°) and a tetrahedron (σ = 109.°). These values are similar to those determined for the solid-state structure of the isoelectronic $HFe(CO)_4^-$.[42] The theoretical analysis of metal carbonyl fragments by Elian and Hoffmann[39] places the hydride ligand in the axial position of a trigonal bipyramid and predicts the highest stability for the C_{3v} geometry at $\theta >$ 95°.

The Co-H distance of 1.56 Å is close to that reported for diatomic hydride, (CoH), at 1.593 Å.[43] The equatorial oxygens are bent toward the hydrogen atom and more closely approx-

Table IV. Bond Lengths (Å) in $XM(CO)_4$ Complexes

Compound	Technique	X-M	C-O(av)	M-C_{ax}	M-C_{eq}	Ax − eq	C_{ax}-M-C_{eq}[0]	Eq plane to M	Ref
$H_3SiCo(CO)_4$	Electron	2.381 (7)	1.137 (3)	1.802 (3)[a]	1.802 (3)[a]	0.0	98.3 (6)	—	47
$F_3SiCo(CO)_4$	X-ray	2.226 (6)	1.12 (2)	1.80 (2)	1.78 (1)	0.02	94.4 (8)	—	48
$Cl_3SiCo(CO)_4$	X-ray	2.254 (3)	1.147 (9)	1.797 (9)	1.767 (5)	0.03	94.8 (5)	0.15	49
$HFe(CO)_4^-$	X-ray	1.57 (12)	1.155 (3)	1.72 (2)	1.75 (2)	−0.03	98.4 (7)	0.27	42
$HCo(CO)_4$	Electron	1.55 (1)	1.141 (3)	1.764 (10)	1.818 (3)	−0.05	99.7 (3)	0.30	This work

[a] Assumed equal.

imate a tetrahedron than do the carbons. The H···C_{eq} distance is 2.12 Å, about halfway between the covalent and van der Waals radius. The axial Co-C bond is 0.051 Å shorter than the equatorial Co-C bonds, which is four times the combined estimated errors, and in a direction opposite to that found for $H_2Fe(CO)_4$, even though in magnitude these M-C bonds are quite close. Note, however, that in a d^8 trigonal bipyramid, the axial bonds are predicted to have a stronger σ contribution, although π bonding is stronger at the equatorial sites.[44] In $Fe(CO)_5$ the axial bonds are shorter by 0.02 Å.[30] The distance from the plane of the three equatorial carbons to the cobalt is 0.306 Å. These values are also similar to the solid-state structure for the isoelectronic $HFe(CO)_5^-$.[42] A comparison of the best model with related compounds is presented in Table IV.

The majority of the scattering from these molecules in the gas phase is due to M—C, C—O and M···O, while that due to C···C, C···O, and O···O is comparatively small. For the latter individual atom pairs the l_{ij}'s reflect the thermally populated modes of vibration. The bending modes for C···C, C···O, and O···O are low in energy. Their l_{ij}'s are undoubtedly affected by the temperature of the sample in the gas phase. Because of the variation in temperature for the three gas samples any comparison of their l_{ij}'s associated with the low-frequency bending modes is difficult. However, for the l_{ij}'s associated with each particular molecule some notable trends do occur. For the $HMn(CO)_5$ and $HCo(CO)_4$ the mean amplitudes of vibration for C_{ax}···C_{eq} are less than C_{eq}···C_{eqbase}. For $H_2Fe(CO)_4$ the mean amplitudes of vibration for the two internal angles τ_1 and τ_2 are equal within the combined error limits. Although assigned vibrational data for the low-frequency bending modes are not available, the l_{ij}'s listed are the right order of magnitude for $\nu \cong 100$ cm^{-1}.

In all the metal hydride structures the shrinkage corrections could not be calculated with much precision and have, therefore, been set to zero. For some of the longer distances this may result in changes up to 0.02 Å. By varying the weighting scheme and the differences between axial and equatorial CO bond lengths and changing values for the shrinkage corrections, the ability to differentiate between chemically distinct bond lengths becomes difficult. When two distinct bonds differ by less than their vibrational amplitudes electron diffraction techniques may not be able to distinguish these fine details.

These three molecules confirm that the hydrogens in transition metal hydrides are definitely stereochemically active. The $Co(CO)_4$ and $Fe(CO)_4$ fragments are distorted from T_d symmetry. The average M-C and M-H distances decrease from manganese to cobalt, as do the central metal radii. Photoelectron spectra[45,46] show that the ionization potentials for the M-H bonding orbitals increase from manganese to cobalt, in agreement with the observed trend in interatomic distances. The carbonyls introduce a minimum of ligand-ligand repulsion, so that the distortions in these compounds should reflect the electronic structures of the central metal atom. Indeed, the observed distortions have been explained by Hoffmann[39] in terms of the electronic structure of the central atom. These experimental results agree quite well with his conclusions.

Acknowledgments. The authors gratefully acknowledge discussions with Professors Simon Bauer and Roald Hoffmann, and E.A.M. thanks Cornell University for a graduate fellowship. It is with deepest regret that F.R.S. must announce the untimely death of his former graduate student and coauthor Edward McNeill. He is sorely missed by both chemists and friends alike.

References and Notes

(1) W. Hieber and F. Leutert, *Naturwissenschaften*, **19**, 360 (1931); G. W. Coleman and A. A. Blanchard, *J. Am. Chem. Soc.*, **58**, 216 (1936).
(2) S. J. La Placa, W. C. Hamilton, J. A. Ibers, and A. Davison, *Inorg. Chem.*, **8**, 1928 (1969).
(3) R. V. G. Ewens and M. W. Lister, *Trans. Faraday Soc.*, **35**, 681 (1939).
(4) W. F. Edgell, C. Magee, and G. Gallup, *J. Am. Chem. Soc.*, **78**, 4185 (1956); G. Bor, *Inorg. Chim. Acta*, **1**, 82 (1967).
(5) A. P. Ginsberg, *Transition Met. Chem.*, **1**, 146 (1965).
(6) M. L. Green and D. J. Jones, *Adv. Inorg. Chem. Radiochem.*, **7**, 126 (1965).
(7) K. Farmery and M. Kilner, *J. Chem. Soc. A*, 634 (1970).
(8) G. F. Bradley and S. R. Stobart, *J. Chem. Soc., Chem. Commun.*, 325 (1975).
(9) D. K. Huggins and H. D. Kaesz, *J. Am. Chem. Soc.*, **86**, 2734 (1964).
(10) T. C. Farrar, W. Ryan, A. Davison, and J. W. Faller, *J. Am. Chem. Soc.*, **86**, 184 (1966).
(11) T. C. Farrar, F. E. Brinkman, T. D. Doyle, A. Davison, and J. W. Faller, *Inorg. Chem.*, **6**, 161 (1967).
(12) J. H. Van Vleck, *Phys. Rev.*, **74** 1168 (1948).
(13) D. L. Van der Hart, H. S. Gutowsky, and T. C. Farrar, *J. Am. Chem. Soc.*, **89**, 5056 (1967).
(14) G. M. Sheldrick, *Chem. Commun.*, 751 (1967).
(15) A. G. Roblette, G. M. Sheldrick, and R. N. F. Simpson, *J. Mol. Struct.*, **4**, 221 (1969).
(16) S. J. La Placa, W. C. Hamilton, and J. A. Ibers, *Inorg. Chem.*, **3**, 1491 (1964).
(17) Discussion of structural techniques and conclusions drawn are outlined by B. A. Frenz and J. A. Ibers in "Transition Metal Hydrides", E. L. Muetterties, Ed., Marcel Dekker, New York, N.Y., 1971, p 33.
(18) S. H. Bauer and K. Kimura, *J. Phys. Soc. Jpn.*, **17**, 300 (1962).
(19) Kodak Electron Image Plates used at maximum speed. HRP (1:2). See Kodak Information Pamphlet KPØ57754a-66.
(20) R. L. Hilderbrandt and S. H. Bauer, *J. Mol. Struct.*, **3**, 325 (1969).
(21) L. Schafer, A. C. Yates, and R. A. Bonham, *J. Chem. Phys.*, **55**, 3055 (1971).
(22) J. L. Carlos, Thesis, Cornell University, 1972.
(23) E. A. McNeill, Ph.D. Thesis, Cornell University, 1975.
(24) A. L. Andreassen, D. Zebelman, and S. H. Bauer, *J. Am. Chem. Soc.*, **93**, 1148 (1971).
(25) W. Harshbarger, G. Lee, R. F. Porter, and S. H. Bauer, *Inorg. Chem.*, **8**, 1683 (1969).
(26) S. H. Bauer and A. L. Andreassen, *J. Phys. Chem.*, **76**, 3099 (1972).
(27) F. A. Cotton and G. Wilkinson, "Advanced Inorganic Chemistry", Wiley, New York, N.Y., 1972, p 705.
(28) H. W. Stelnberg, I. Wender, R. A. Friedel, and M. Orchin, *J. Am. Chem. Soc.*, **75**, 2717 (1953).
(29) B. Beagley and D. G. Schmidling, *J. Mol. Struct.*, **22**, 466 (1974).
(30) B. Beagley and D. W. J. Cruickshank, *Acta Crystallogr., Sect. B*, **29**, 1499 (1973).
(31) R factor = $|I_{obsd} - I_{calcd}|/I_{calcd}$; I_{obsd} = observed intensity, I_{calcd} = calculated intensity.
(32) W. C. Hamilton, *Acta Crystallogr.*, **18**, 502 (1965).
(33) L. F. Dahl and R. E. Rundle, *Acta Crystallogr.*, **16**, 419 (1963).
(34) P. A. Agron, R. D. Ellison, and H. A. Levy, *Acta Crystallogr.*, **23**, 1079 (1967).
(35) H. M. Seip and R. Seip, *Acta Chem. Scand.*, **24**, 3431 (1970).
(36) D. W. H. Rankin and A. Robertson, *J. Organomet. Chem.*, **88**, 181 (1975).
(37) M. J. Bennett and R. Mason, *Nature (London)*, **205**, 760 (1965).

(38) A. D. Berry, E. R. Corey, A. P. Hagen, A. C. MacDiarmid, F. E. Saalfeld, and B. F. Wayland, *J. Am. Chem. Soc.*, **92**, 1940 (1970).
(39) M. Elian and R. Hoffmann, *Inorg. Chem.*, **14**, 1058 (1975).
(40) L. J. Guggenberger, D. D. Titus, M. T. Flood, R. E. Marsh, A. A. Orlo, and H. B. Gray, *J. Am. Chem. Soc.*, **94**, 1135 (1972).
(41) M. Poliakoff and J. J. Turner, *J. Chem. Soc., Dalton Trans.*, 2276 (1974).
(42) M. B. Smith and R. Bau, *J. Am. Chem. Soc.*, **95**, 2388 (1973).
(43) G. Herzberg, "Spectra of Diatomic Molecules", 2nd ed, Van Nostrand, New York, N.Y., 1950, p 522.
(44) A. R. Rossi and R. Hoffmann, *Inorg. Chem.*, **14**, 365 (1975).
(45) S. Cradock, E. A. Ebsworth, and A. Robertson, *J. Chem. Soc., Dalton Trans.*, 22 (1973).
(46) M. F. Guest, B. R. Higginson, D. R. Lloyd, and I. H. Hillier, *J. Chem. Soc., Faraday Trans. 2*, **70**, 902 (1975).
(47) A. G. Roblette, G. M. Sheldrick, R. N. F. Simpson, B. J. Aylett, and J. A. Campbell, *J. Organomet. Chem.*, **14**, 279 (1968).
(48) K. Emerson, P. R. Ireland, and W. T. Robinson, *Inorg. Chem.*, **9**, 436 (1970).
(49) W. T. Robinson and J. A. Ibers, *Inorg. Chem.*, **8**, 1208 (1967).

Zero-Coordinate K^+. Crystal Structure of Dehydrated Cesium and Potassium Exchanged Zeolite A, Cs_7K_5-A

Roger L. Firor and Karl Seff*

Contribution from the Chemistry Department, University of Hawaii, Honolulu, Hawaii 96822. *Received October 19, 1976*

Abstract: The structure of vacuum-dehydrated $Cs_7K_5Al_{12}Si_{12}O_{48}$, zeolite A with all Na^+ ions replaced by Cs^+ and K^+ as indicated, has been determined by single-crystal x-ray diffraction techniques in the cubic space group $Pm3m$ (a = 12.266 (2) Å). The final weighted R index is 0.047. In the structure, three Cs^+ ions fill an equipoint at the very centers of the oxygen 8-rings. Three other equivalent Cs^+ ions and three equivalent K^+ ions occupy respective equipoints on threefold axes opposite 6-rings in the large cavity. The three remaining cations lie on one unique threefold axis. Two of these, the Cs^+ ion and one K^+ ion, are located in the sodalite unit on opposite sides of the origin. *The remaining K^+ ion on this threefold axis is 4.40 Å from its nearest neighbors, three 6-ring oxide ions. This K^+ ion lies deep within the large cavity and can be considered zero coordinate by a distance criterion; its shortest approach to another ion exceeds the sum of the appropriate ionic radii by more than 1.7 Å.* This situation has occurred because insufficient sites are available on the inner surface of the zeolite to accommodate all of the large cations present. By difference, one cation per unit cell, in this case K^+, must occupy a site remote from the anionic zeolite framework.

Zero-coordinate, large monovalent cations were observed in the crystal structures of dehydrated K_{12}-A[1,2] and $Rb_{11}Na_1$-A.[2,3,4] In dehydrated K_{12}-A,[1] one K^+ ion per unit cell was located deep within the large cavity, 4.25 Å from its nearest neighbors, three framework oxide ions of a 6-ring.[5] In dehydrated $Rb_{11}Na_1$-A,[3,4] one Rb^+ ion per unit cell occupies a similar position 4.35 Å from the 6-ring oxide ions. The closest ionic contacts of these monovalent cations to framework oxide ions are too long by at least 1.5 Å.[6] The term "zero coordination"[3,4] is employed to describe this discrepancy.

In this work, the third zeolite A crystal structure to contain a zero-coordinate cation is reported. Initial hopes that a higher degree of Cs^+ exchange would be attained, and that the zero-coordinate cation would be Cs^+, have not been realized. Nevertheless, the result reconfirms the existence of uncoordinated cations, K^+ in this case, and demonstrates again the conditions[3,4] necessary for their occurrence.

Experimental Section

Crystals of zeolite 4A were prepared by a modification of Charnell's method,[7] including a second crystallization using seed crystals from the first synthesis. A single crystal 0.085 mm on an edge was lodged in a fine glass capillary. The crystal was first exchanged with 0.2 N KOH (Mallinckrodt, Analytical Reagent: Na^+, 0.05%; NH_4^+, 0.02%; all other cations, less than 0.01%) by flow methods—a continuous stream of fresh solution flowed past the crystal at a velocity of approximately 1.0 cm/s for a period of 2 days at 25 (1) °C. Next, the crystal was similarly exchanged with 0.1 N CsOH (Ventron/Alfa, 99.9% purity) for 12 days. After the solution was drained, no noticeable droplet of solution remained close to the crystal, and a rinse step, which might have caused some H^+ exchange, was not performed. After dehydration at 350 °C and 2×10^{-6} Torr for 48 h, the crystal was allowed to cool to room temperature, and was sealed in its capillary, while still under vacuum, by torch. The microscopic appearance of the crystal was not altered by these exchange and dehydration procedures.

The dehydrated zeolite, with a unit cell composition of $Cs_7K_5Si_{12}Al_{12}O_{48}$ as determined by refinement of the diffraction data, will subsequently be referred to as Cs_7K_5-A.

X-Ray Data Collection. The space group $Pm3m$ (no systematic absences) was used throughout this work for reasons discussed previously.[8,9] Preliminary crystallographic experiments and subsequent data collection were performed with an automated, four-circle Syntex $P\bar{1}$ diffractometer, equipped with a graphite monochromator and a pulse-height analyzer. Molybdenum radiation was used for all experiments ($K\alpha_1$, λ = 0.70930 Å; $K\alpha_2$, λ = 0.71359 Å). The cubic unit cell constant, as determined by a least-squares refinement of 15 intense reflections for which $2° < 2\theta < 24°$, is 12.266 (2) Å.

Reflections from two intensity-equivalent regions of reciprocal space (hkl, $h \leq k \leq l$, and lhk, $l \leq h \leq k$) were examined using the θ–2θ scan technique. Each reflection was scanned at a constant rate of 1.0 deg min^{-1} from 0.8° (in 2θ) below the calculated $K\alpha_1$ peak to 0.8° above the $K\alpha_2$ maximum. Background intensity was counted at each end of a scan range for a time equal to half the scan time. Other details of the data collection and reduction[10] are the same as previously described.[4] No absorption correction was applied to the data. Of the 881 pairs of reflections examined for Cs_7K_5-A, only the 314 whose net counts exceeded three times their corresponding esd's were used in structure solution and refinement.

Structure Determination. Full-matrix least-squares refinement of the structure was initiated using the atomic parameters for the framework atoms ((Si,Al), O(1), O(2), and O(3)) and for Cs^+ which had previously been found in the crystal structure of Cs_7Na_5-A.[11] Anisotropic refinement of all ions, except those at Cs(1) and Cs(3) which remained isotropic, converged quickly to an R_1 index, $(\Sigma||F_o| - |F_c||)/\Sigma F_o$, of 0.154 and a corresponding weighted R_2 index, $(\Sigma w(F_o - |F_c|)^2/\Sigma w F_o^2)^{1/2}$, of 0.187. (Refer to Table I and Figure 2 to identify these positions.) Simultaneous occupancy and thermal